IRAQI JOURNAL OF APPLIED PHYSICS
Vol. 22, No. 2, April-June 2026, pp. 260-267

Preparation of Cu@AgI Core–Shell Nanocolloid via Pulsed Laser Ablation for Enhanced Al/Cu@AgI/Si/Al Photodetector Performance

Hafsa T. Ahmed *
Aliaa M. Alwan
Hanan R. Abd Ali

Department of Physics,
College of Education for
Pure Sciences,
University of Tikrit,
Tikrit, IRAQ
* Corresponding author email:
hafsa.t.ahmed@tu.edu.iq

This study seeks to synthesize Cu@AgI core-shell structures by laser ablation to fabricate high-performance Al/Cu@AgI/Si/Al photodetectors. The XRD results revealed that the AgI sample displayed diffraction peaks corresponding to silver iodide and silver oxide. The mean crystallite sizes were 28.08 nm for AgI and 31.28 nm for the core-shell structure. The particles had a quasi-spherical morphology, with a minimum diameter of 37.99 nm. The energy bandgap was 2.85 eV for AgI and 2.68 eV for Cu@AgI. The FTIR spectra indicated no notable alterations in the Cu@AgI core-shell structure, indicating the absence of lattice vibrations for AgI in the mid-IR. The Al/Cu@AgI/Si/Al photodetectors demonstrated peak specific detection at 450 nm and 900 nm, with quantum efficiency rising from 48.83% to 80.74%.

Keyword: Silver iodide; Core-Shell; Pulsed-Laser Ablation in Liquid; Photodetectors
Received: 13 August 2025; Revised: 19 October 2025; Accepted: 26 October; Published: 1 April 2026

1. Introduction

Nanomaterials play a vital role in both the advancement and use of nanotechnology. When a particle's size is diminished, various effects manifest, including small size, surface, quantum size, and quantum tunneling effects. Due to these effects, materials show a variety of macroscopic characteristics. The basic function of the detector is to absorb light and generate an electron-hole pair [1]. They are enhanced by smaller nanoparticles, which have a higher surface-to-volume ratio. In recent years, there has been considerable interest in the applications of copper (Cu) and Cu-based nanoparticles, which are derived from the inexpensive and abundantly available copper metal. By enhancing charge transport and reducing electron-hole recombination, copper nanoparticles (CuNPs) significantly boost the efficiency of photodetectors in optoelectronic devices. In recent years, thanks to innovation in materials science and its integration with semiconductor technology, there has been significant development in optical detectors. Recent studies underscore various substantial advancements that yield superior performance and broaden the range of industrial applications. Due to their unique optical properties, gold (Au), silver (Ag), and copper (Cu) nanoparticles are particularly interesting for plasmonic applications. AuNPs exhibit a strong and tunable LSPR that spans from the visible to the near-infrared range. This trait renders them highly appropriate for sensing, imaging, and photothermal therapy. Nonetheless, CuNPs offer a cost-effective alternative with similar plasmonic properties, particularly useful in catalysis and solar energy capture, despite being less stable than gold [2-4]. Special interest is drawn to semiconductor nanoparticles like silver iodide (AgI) as they occupy an intermediate state between atoms, molecules, and bulk materials, making it likely that they possess exceptional properties. The study of AgI has led to advancements in solid-state ionics, photography, and the use of related devices. Therefore, it is essential to design and control the synthesis of nanostructures. Due to its superionic α-phase and high Ag^+ conductivity, AgI is a remarkable compound. AgI possesses a direct band gap of approximately 2.9 eV and typically consists of a combination of β-AgI and γ-AgI at room temperature. AgI exists in the α-phase above 147°C, which exhibits superionic behavior that has been extensively studied [5,6]. The superionic conductor that has been studied the most is AgI. The highly disordered structure of the phase was attributed to its ionic conductivity. A comprehensive specialized study was conducted to determine how size affects phase transition temperature and ionic conductivity. Nano silver iodide (AgI) serves multiple purposes, such as in photocatalysis, sensors, and rapid ionic conductors. Due to its exceptional conductivity and distinctive photoelectrical characteristics, AgI is a material with great promise for use in commercial applications. Methods currently used to prepare nano AgI include precipitation reaction, laser ablation, reverse microemulsion, and ultrasonic spray pyrolysis [6,7]. Pulsed-laser ablation (PLA) of nanoparticles offers numerous benefits compared to traditional methods; this technique is cost-effective and can produce pure nanoparticles with good control of size and shape. It allows for the synthesis of core–shell nanocomposites while preserving stoichiometry, and it offers a short reaction time [8-10].

This study aimed to synthesize Cu@AgI core-shell

nanoparticles for evaluation of their detection capacity. The results indicated that the Cu@AgI nanoparticles exhibit excellent performance. To our knowledge, this work using Cu@AgI is significant for the development of photodetectors.

2. Experimental Part

AgI and Cu@AgI nano-colloids were prepared using the pulsed-laser ablation in liquid (PLAL) method. The system utilized a Q-switched Nd:YAG laser (Quanta-Ray, 1064 nm) operating at a frequency of 5 Hz. The schematic representation of the mechanisms that occur in the PLAL method is shown in Fig. (1).

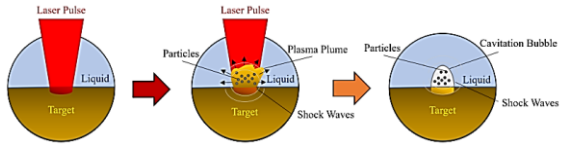

Fig. (1) Schematic representation of the mechanisms that occur in the PLAL method

For the synthesis of AgI and Cu nanoparticles, a highly pure (99.99%) silver iodide (AgI) pellet and a highly pure copper (Cu) pellet (see Fig. (2) for the targets) were used as targets, respectively. The targets were submerged into 10 mL of deionized water inside a cylindrical glass cell at room temperature (34°C).

(a) (b) (c)

Fig. (2) From left (a) pellet of AgI, (b) pellet of copper, (c) water, Cu NPs and AgI@Cu)

The laser beam was focused onto the pellet surface using a converging lens with a 12 cm focal length. The target was submerged 1 cm deep in deionized water. The pulse energy was set at 400 mJ at the target, with a pulse duration of 7 ns, resulting in a laser spot diameter of approximately 1 mm and a calculated laser fluence (energy density) of approximately 10 J/cm^2. A total of 400 pulses were applied for 15 min for each target.

The 15-min ablation time was chosen based on preliminary studies to achieve an optimal visual concentration and particle size distribution. The resulting colloid concentration was monitored by measuring the optical density (OD) at a reference wavelength of 500 nm to ensure batch consistency and reproducibility.

To prepare the Cu@AgI core-shell structure, the AgI pellet was ablated first for 15 min to obtain the AgI nano-colloid. Then, a highly pure Cu target was ablated inside the previously prepared AgI nano-colloid solution for another 15 min. This two-step process facilitates the formation of the Cu core encapsulated by the AgI shell. All syntheses were performed in triplicate to ensure reliability and repeatability.

The photodetector device, labeled Al/Cu@AgI/Si/Al (consistent nomenclature), was fabricated on n-type (100) silicon wafer (with a resistivity of 1-10 Ω.cm and a thickness of 300 µm). The schematic of the photodetector fabrication process is shown in Fig. (3).

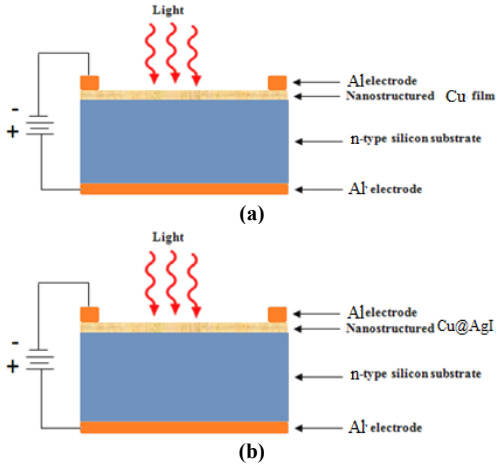

Fig. (3) Schematic diagrams of the photodetector fabrication process (a) Cu/Si, and (b) AgI@Cu/Si)

The silicon wafer was cleaned using the standard RCA method (Radio Corporation of America) to remove organic and inorganic contaminants. An aluminum (Al) layer with a thickness of 500 nm was thermally evaporated onto the back surface of the Si wafer to form a uniform Ohmic contact. The synthesized Cu@AgI nano-colloid was deposited onto the clean front surface of the Si wafer using the drop-casting technique. A final top contact of aluminum (Al) was thermally evaporated onto the Cu@AgI layer through a metallic mask to create active area electrodes of 2 cm^2. The final structure of the photodetector was Al/Cu@AgI/Si/Al.

The structural, morphological, optical, and electrical properties of the prepared Nano colloids and the fabricated device were analyzed using the following techniques. X-ray diffraction (XRD) analysis was performed to determine the crystalline structure and crystallite size of the prepared AgI and Cu@AgI Nano colloids. Field-emission scanning electron microscopy (FE-SEM) was used to study the surface morphology of the deposited films. Atomic force microscopy (AFM) was utilized to assess the film roughness and particle aggregation size, with the specific intent to clarify in the Discussion section whether the reported values represent lateral size or height and to address tip-convolution effects. The UV-Visible spectrophotometer was used to record the absorption spectra and calculate the optical energy bandgap (E_g). Fourier-transform infrared (FTIR) spectroscopy was used to investigate the chemical bonds and functional

groups. The current-voltage (I-V) characteristics of the fabricated Al/Cu@AgI/Si/Al device were measured using a digital source meter.

3. Results and Discussion

The crystallite structure of the prepared AgI and Cu@AgI nano-colloids was determined by XRD analysis, as shown in Fig. (4). The diffraction peaks observed for AgI were consistent with the gamma phase (γ-AgI), which has a face-centered cubic (FCC) structure, matching JCPDS card 01-078-2434. The stabilization of this γ-phase, which is typically semi-stable at room temperature, is attributed to the non-equilibrium synthesis and rapid plasma cooling inherent to the PLAL technique.

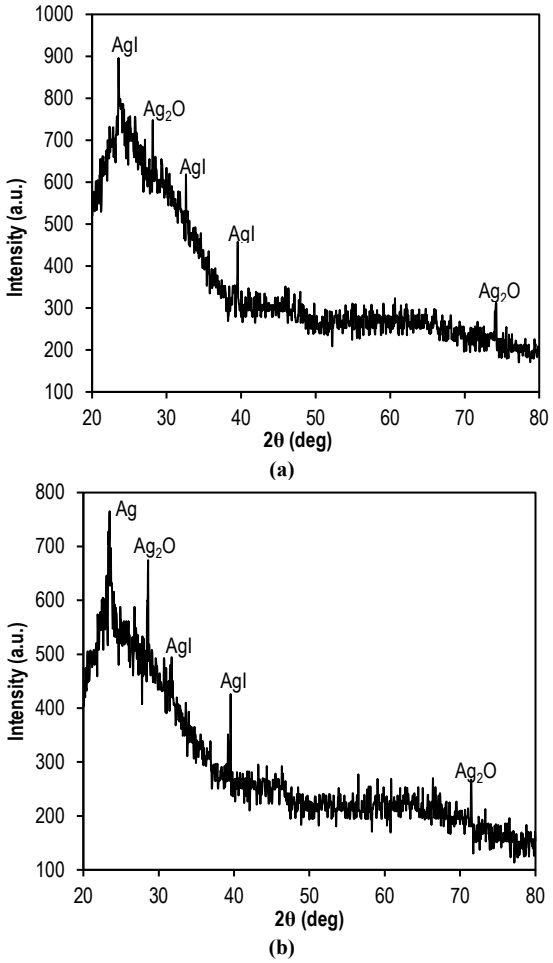

Fig. (4) XRD patterns of (a) AgI and (b) Cu@AgI films

For the Cu@AgI sample, the absence of characteristic Cu peaks supports the core-shell structure, indicating the copper core is effectively encapsulated by the AgI shell, which hinders the X-rays from diffraction.

The XRD analyses confirmed the presence of AgI and Miller (hkl) planes of AgI (002), (102), and (110) at positions of 2θ= 23.45°, 32.59°, and 39.58°. It is noted that the peak at 28.14° and 74.21° with miller (hkl) planes (311) and (201) are corresponding to silver oxide (ICDD card 19-1155). Figure (4b) presents XRD patterns for Cu/AgI core-shell. The peaks at 2θ= 23.49°, 32.01°, and 39.54° indicate the presence of AgI, while those at 2θ= 26.99°, 28.59°, and 74.19° signify the presence of Ag_2O. There were no detected Cu peaks. The lack of copper peaks in the diffraction pattern indicates that all copper atoms are shielded and have formed Cu@AgI core–shell nanoparticles. The lack of diffraction peaks from the copper core atoms indicates that these atoms are in a kinematic diffraction state, which is why only the shell metallic peaks are observed [14,15]. The synthesized nanoparticles have completely formed as core–shell nanostructures in the reaction medium, as evidenced by this XRD pattern. Using the Scherrer's formula (Eq. 1), the average crystallite size was determined to be approximately 39.72 nm for AgI and 31.72 nm for the AgI@Cu core-shell.

$$D = \frac{0.9\lambda_{x-ray}}{\beta cos\theta} \qquad (1)$$

where β is the full-width at half maximum (FWHM) and θ is the diffraction angle [16]

Table (1) provides an overview of the most important parameters obtained from the XRD patterns of AgI and AgI@Cu samples.

AFM images of AgI and Cu@AgI NPs deposited on glass substrates are shown in Fig. (5). The average diameters of AgI nanoparticles (Fig. 3a) are 95.14 nm. The average diameter of the Cu@AgI core-shell nanoparticles (Fig. 3b) is 142 nm, which exceeds the diameters of the AgI nanoparticles, suggesting that copper nanoparticles are enveloped by a silver iodide shell. The surface roughness increased from 9.59 nm to 15.48 nm with the Cu core present, which can be linked to an increase in height (along the z-axis) due to a higher volume ratio of nanoparticles. In certain regions of the coated film, aggregation of large nanoparticles has been observed, indicating a potential increase in series resistance within this film [17].

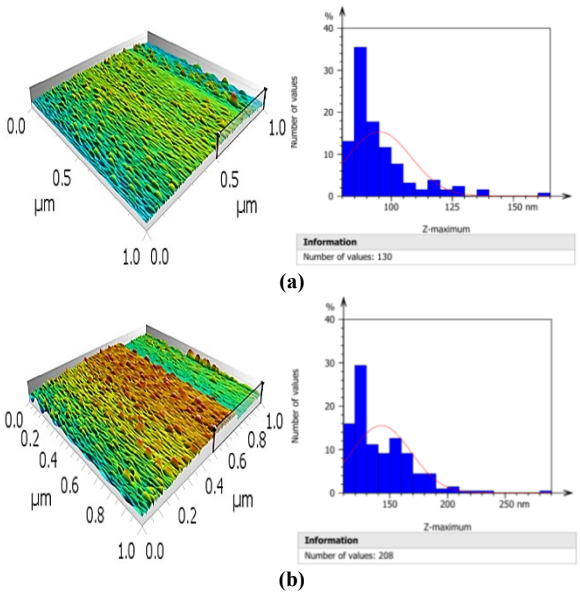

Fig. (5) AFM results of (a) AgI and (b) Cu@AgI films

Film samples of the produced AgI and Cu@AgI nanoparticles were subjected to FE-SEM analysis in order to evaluate the morphological structure of the produced nanoparticles. The AgI NPs (Fig. 6a) were semi-spherical, with the smallest diameter of AgI nanoparticles being approximately 31.64 nm. The images clearly show a large aggregate of small spherical particles, as well as some irregularly shaped particles of various sizes. This clustering may be explained by the van der Waals force between the particles [18]. Figure (6b) presents an FE-SEM image of the synthesized Cu@AgI nanoparticles, which form a cluster-like structure with varying sizes, showing a reasonably homogenous distribution. The combination of sphere- and semi-sphere-shaped particles results in a more regular arrangement, and the particle diameter of AgI (with the smallest diameter of 37.99 nm) increases after adding the Cu core compared to AgI without it. This may be due to the expansion of the AgI shell in the presence of the Cu core.

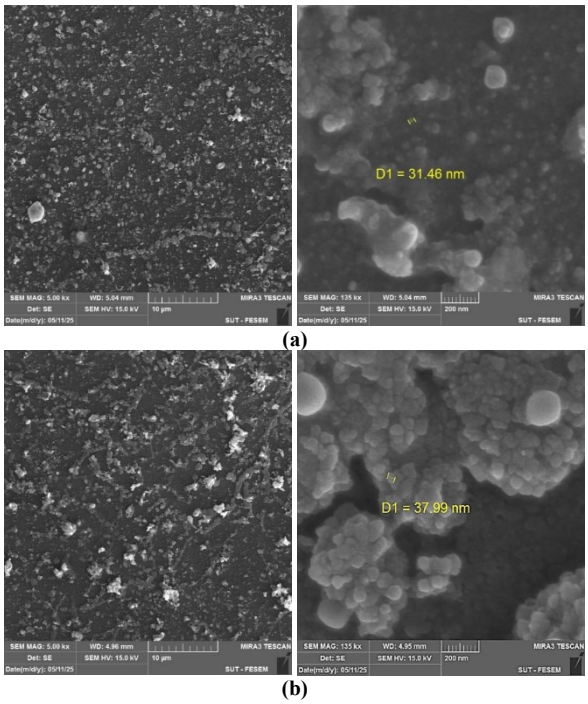

Fig. (6) FE-SEM images of the synthesized (a) AgI and (b) Cu@AgI films

The formation of this agglomerate suggests that the surface energy of the nanoparticles is quite strong. Optical properties like absorption coefficient are crucial in photodetector materials, as the bandgap value significantly influences photodetector performance. The optical absorption spectra of noble metal nanoparticles are known to consist of strong peaks resulting from plasmon excitations. Consequently, we measured the UV-visible absorption spectra of the as-prepared AgI and core-shell nanoparticles, and the outcome is illustrated in Fig. (7). Figure (7a) displays the UV-visible absorption spectra of a produced yellowish-white solution of AgI NPs, with an absorption peak at 426 nm in the visible range. Clearly, the absorption band of AgI aligns well with that reported in previous studies on AgI nanoparticles [19]. The absorption peak of Cu@AgI was broadened, and its intensity decreased. A decrease in absorbance has been noted for Cu@AgI core-shell synthesized in aqueous medium, which is attributed to the reduction of Ag and Cu nanoparticle content and the probable formation of CuO/Ag_2O during synthesis. For AgI@Cu core-shell nanoparticles, the absorption edge exhibited a red shift in relation to the absorption spectra. This observation is attributed to the increase in particle sizes resulting from the formation of core-shell nanoparticles [20]. Tauc's relationship is used to calculate the optical band gap (E_g) of the prepared particles (AgI NPs) [21]. The energy band gap values for the synthesized AgI NPs were established by plotting $(\alpha h\upsilon)^n$ against photon energy ($h\upsilon$). Bandgap values for Cu@AgI were derived using the direct-allowed transition model ($(\alpha h\nu)^2$) as

$$\alpha h\upsilon = A(h\upsilon - E_g)^{\frac{1}{2}} \qquad (2)$$

where α is the absorption coefficient, $h\upsilon$ is the photon energy, E_g is the energy bandgap, and A is a constant

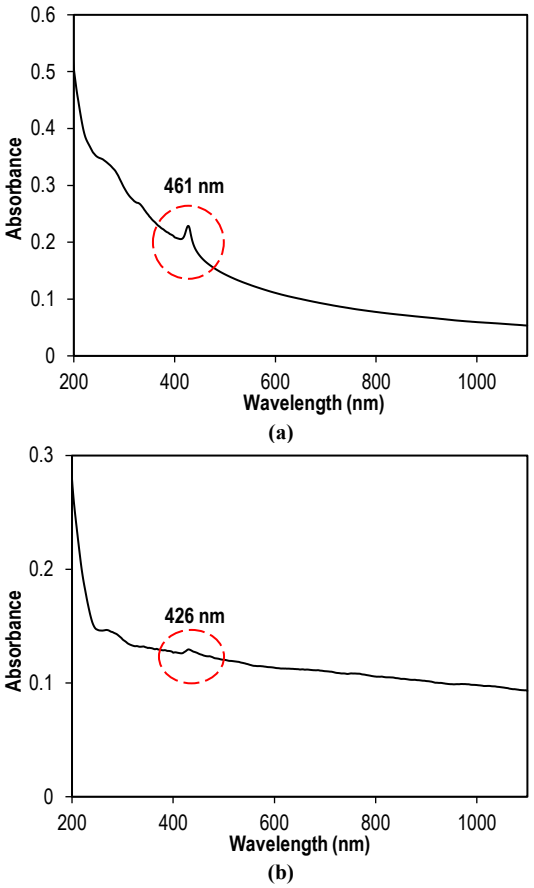

Fig. (7) UV-visible absorption spectra of (a) AgI and (b) Cu@AgI colloids

As illustrated in Fig. (8), the energy bandgap of AgI was measured at 2.85 eV, while that of Cu@AgI NPs was 2.68 eV. The ongoing reduction of bandgap energies following shell growth around the core nanoparticles may be linked to particle size, which increases after shell formation. Moreover, the reduction

of bandgap energies after surface modification of core nanoparticles is due to the formation of interstitial sites that generate new energy levels (impurity energy levels) between the valence and conduction bands. Furthermore, figure (9) illustrates that the transmittance value of core-shell Cu@AgI decreases from the visible region to the IR region compared to AgI due to an increase in light scattering resulting from its rougher surface morphology.

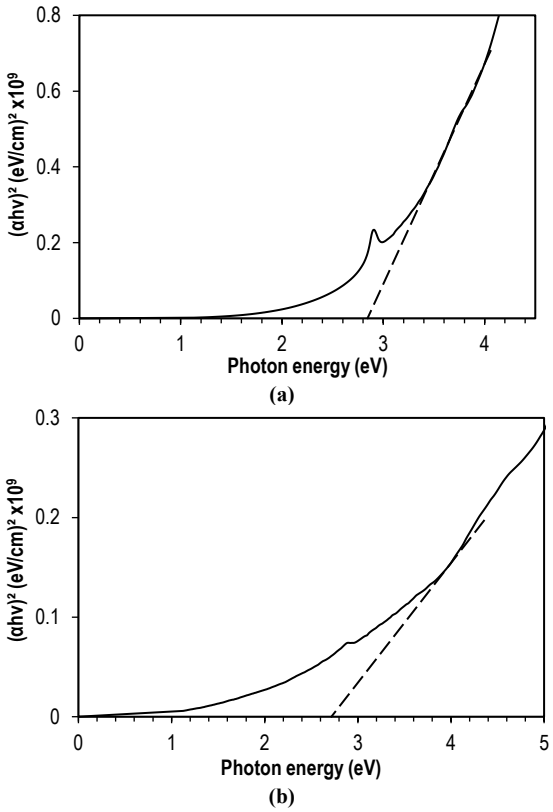

Fig. (8) Tauc relationships to determine energy bandgap of (a) AgI and (b) Cu@AgI nanoparticles

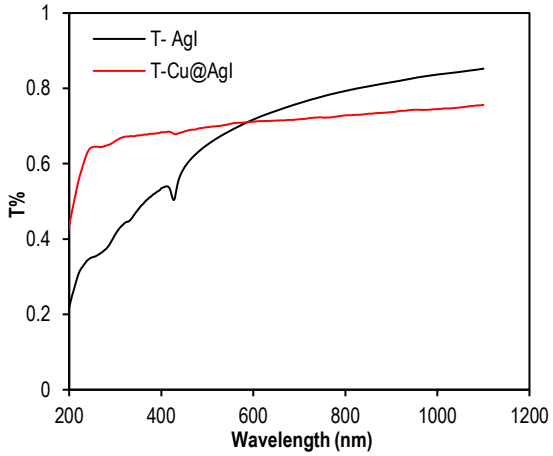

Fig. (9) Transmission spectra of AgI and Cu@AgI) colloids

Figure (10) shows the FTIR spectra of AgI and Cu@AgI core-shell samples. The pronounced peaks seen at 3440-3439 and 1633 cm^{-1} are associated with the stretching vibrations of the OH group, indicating that surface-adsorbed water molecules or hydroxyl (OH^-) groups are present in both samples. The absorption peaks at 2925 and 2854 cm^{-1} were attributed to the stretching of C-H bonds in the methyl group. The wide peaks at 1385 and 1118 cm^{-1} are attributed to C-H and C-O, respectively [22,23]. Additionally, there were no absorption bands observed in the 4000-900 cm^{-1} range associated with AgI, indicating the absence of lattice vibrations for AgI in the mid-IR [6]. When Cu@AgI core-shell was formed, the FTIR spectrum exhibited no substantial alterations relative to the AgI sample; just a minor spectral shift suggested restricted interfacial bonding, demonstrating the physical encapsulation of copper by AgI.

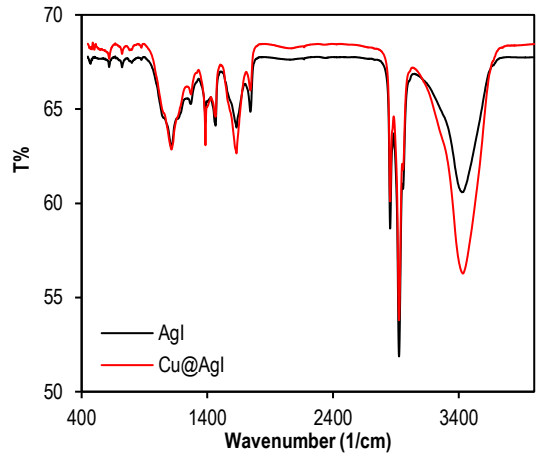

Fig. (10) FTIR spectra of AgI and Cu@AgI colloids

Figure (11) shows the I-V dark characteristics in the forward and reverse directions of Al/Cu/Si/Al and Al/Cu@AgI/Si/Al photodetectors. The forward current of all photodetectors is very small at voltages below 0.5 V. This current is known as the recombination current and occurs only at low voltages. This current is generated when each electron is excited from the valence band to restore equilibrium. The second region at high voltages represents the diffusion or bending region, which depends on the series resistance. In this region, the bias voltage can provide enough energy for the electrons to penetrate the barrier between the two sides of the junction. These results are consistent with those of other researchers [25].

Figure (12) displays the spectral responsivity (using Eq. 3) of Al/Cu/Si/Al and Al/Cu@AgI/Si/Al photodetectors

$$R = \frac{I_{ph}}{P_{in}} \left(\frac{A}{W}\right) \qquad (3)$$

Here, I_{ph} denotes photodetector photocurrent, while P_{in} represents the light power at a given wavelength [24]

The spectral responsivity of Cu/Si within the range of 600-900 nm. The responsivity reaches its peak at λ=600 nm (0.20 A/W), which aligns with the absorption edge of the Cu/Si layer. It should be noted that below the threshold wavelength for Cu absorption, the majority of incident light is absorbed by the Cu layer, leading to the generation and recombination of electron holes within it. The drop in responsivity from 650 to 750 nm may be linked to reduced light

absorption in the Cu layer, leading to a decrease in electron-hole generation [25]. As the wavelength increases to 900 nm, responsivity rises rapidly because of the absorption edge of the Si layer (λ=900 nm, 0.50 A/W).

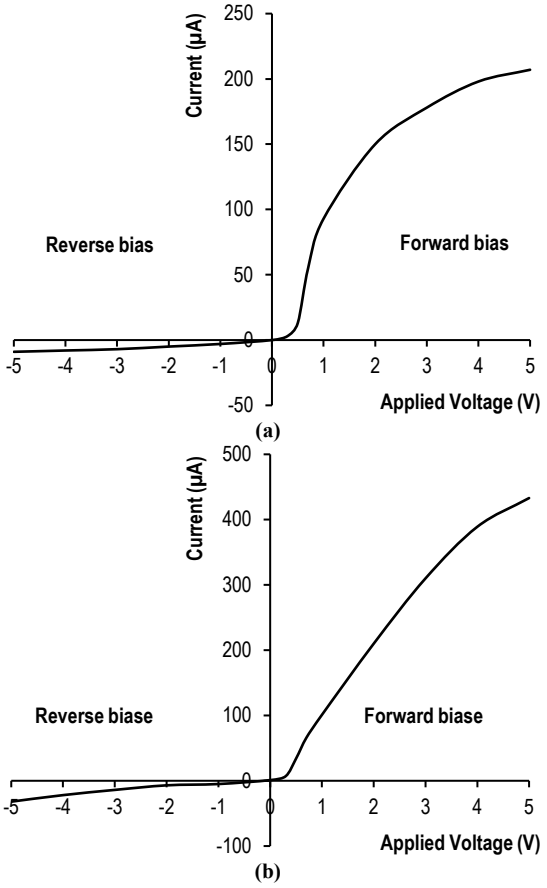

Fig. (11) The I-V characteristics of (a) Al/Cu/Si/Al and (b) Al/Cu@AgI/Si/Al photodetectors

The responsivity of the Cu@AgI core shell was observed at 450 nm, indicating the absorption edge of the silver iodide (as well as silver oxide and silver) particles. This suggests that silver iodide covered the entire copper surface, with copper contributing to an increased response of 0.30 A/W. In other words, the response speed of Cu@AgI/Si is quicker than that of Cu/Si. The responsivity peak seen in the visible region of the Cu@AgI/Si core-shell compared to the Cu/Si device may be due to various factors linked to the unique optical properties of both the copper (Cu) core and the silver iodide (AgI) shell as a novel composite system. Among these factors is the strong localized surface plasmon resonance (LSPR) shown by the silver nanoparticles in the visible region. The LSPR arises when the conduction electrons on the surface of Ag resonate with incident light at certain wavelengths (the collective oscillation of surface electrons), resulting in increased absorption and scattering of light. Furthermore, the LSPR of the copper core can interact with excitonic transitions in the AgI shell. The optical response in the visible region can be enhanced by plasmon-exciton coupling.

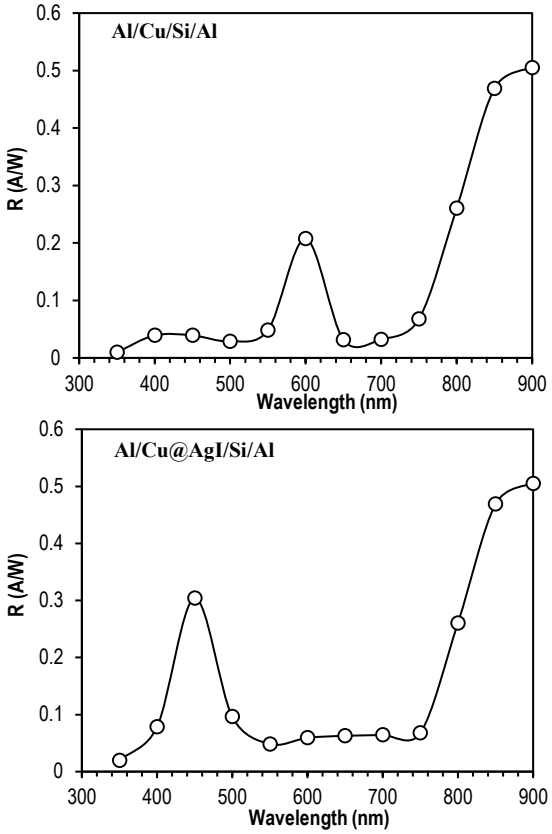

Fig. (12) Spectral responsivity as a function of wavelength for Cu/Si and Cu@AgI/Si photodetectors

The specific detectivity (D^*) of the photodetectors was determined using the following equation [25]:

$$D^* = \frac{R\sqrt{A}}{\sqrt{2qI_d}} \qquad (4)$$

Here, A represents the area of the photodetector, I_d denotes the dark current of the photodetector, and q signifies the charge of an electron [24]

Figure (13) depicts the specific detectivity of the Al/Cu/Si/Al and Al/Cu@AgI/Si/Al heterojunctions. The detectivity values for the Al/Cu/Si/Al device at wavelengths of 600 nm and 900 nm are 2.92×10^{12} Jones and 7.22×10^{12} Jones, respectively. The photodetector's specific detectivity relies on responsivity as well as noise current. Al/Cu@AgI/Si/Al photodetectors exhibit their best specific detectivity at wavelengths of 450 nm, which is 4.34×10^{12} Jones, and 900 nm, which is 7.22×10^{12} Jones.

This study involved calculating the external quantum efficiency (EQE) based on its relationship with the photodetector's wavelength. The EQE of Al/Cu/Si/Al and Al/Cu@AgI/Si/Al heterojunction photodetectors is shown in Fig. (14). It noted that the EQE at wavelengths of 600 nm and 450 nm was 48.83% for Al/Cu/Si/Al and 80.74% for Al/Cu@AgI/Si/Al. The results are ascribed to the creation of electron–hole pairs for every incoming photon [26].

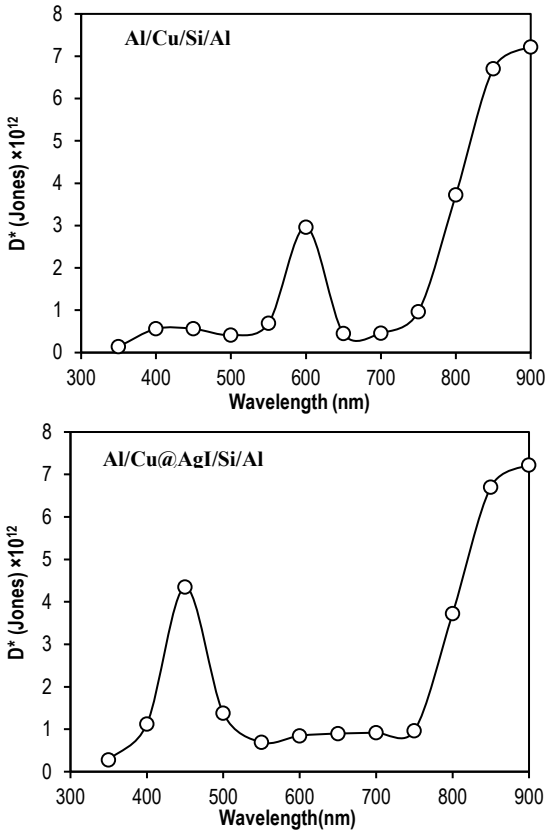

Fig. (13) Specific detectivity as a function of wavelength for Cu/Si and Cu@AgI/Si photodetectors

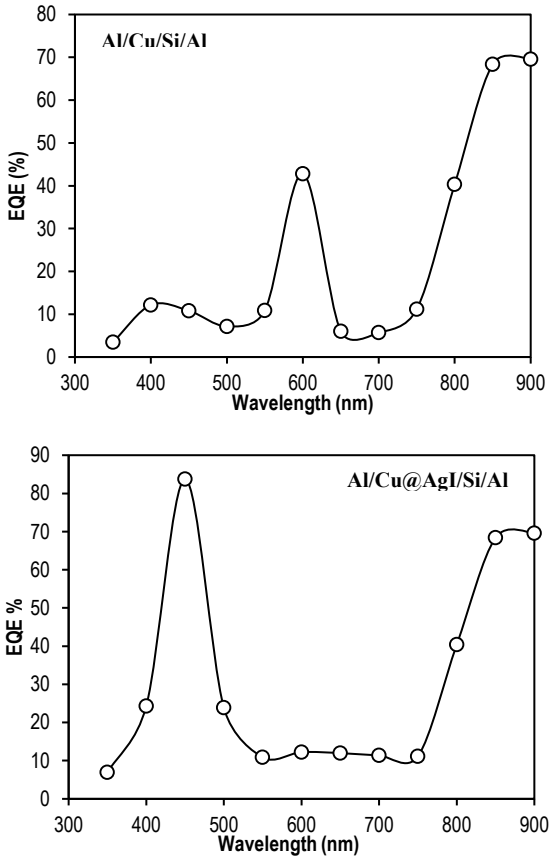

Fig. (14) External quantum efficiency (EQE) as a function of wavelength for Al/Cu/Si/Al and Al/Cu@AgI/Si/Al photodetectors

4. Conclusion

The Al/Cu/Si/Al and Al/Cu@AgI/Si/Al heterojunction photodetectors fabricated in this work show high sensitivity in visible and infrared regions, with response peaks corresponding to the absorption edges of Cu@AgI nanoparticles. Notable detectivity values include 2.92×10^{12} Jones at 600 nm and 7.22×10^{12} Jones at 900 nm for Al/Cu/Si/Al, while Al/Cu/AgI/Si/Al shows optimal detectivity at 450 nm (4.34×10^{12} Jones) and 900 nm (7.22×10^{12} Jones). The external quantum efficiency increased significantly from 48.83% to 80.74%, indicating the potential of Cu@AgI core-shell composites for advanced compact photodetector applications.

References

[1] K.-H. Tseng et al., "A study of preparing silver iodide nanocolloid by electrical spark discharge method and its properties", *Sci. Rep.*, 11(1) (2021) 20457.

[2] M. Gaber et al., "Cu (II) complexes of monobasic bi-or tridentate (NO, NNO) azo dye ligands: Synthesis, characterization, and interaction with Cu-nanoparticles", *J. Mol. Struct.,* 1032 (2013) 185-194.

[3] R.A. Arishi et al., "Gold and Copper Nanoparticles Assisted Porous Silicon for high UV Photodetector Sensitivity by Localized Surface Plasmonic Resonance Phenomena", *Sens. Actuat. A: Phys.,* 390 (2025) 116595.

[4] M.B. Gawande et al., "Cu and Cu-based nanoparticles: synthesis and applications in catalysis", *Chem. Rev.,* 116(6) (2016) 3722-3811.

[5] N.L. Hawari and M.R. Johan, "Synthesis and characterizations of AgI nanoparticles via mechanochemical reaction", *J. Alloys Comp.*, 509(5) (2011) 2001-2006.

[6] R.A. Ismail et al., "Preparation of silver iodide nanoparticles using laser ablation in liquid for antibacterial applications", *IET Nanobiotech.,* 12(6) (2018) 781-786.

[7] X. Wang et al., "One- step hydrothermal synthesis of the Ag/AgI heterojunction with highly enhanced visible- light photocatalytic performances", *Micro Nano Lett.,* 9(6) (2014) 376-381.

[8] D.C. Costa et al., "Laser ablation in liquid-assisted synthesis of three types of nanoparticles for enhanced antibacterial applications", *Int. J. Precis. Eng. Manufact. Green Technol.,* 12 (2025) 1699-1717.

[9] M.S.S. Bharati, B. Chandu and S. Venugopal Rao, "Explosives sensing using Ag–Cu alloy nanoparticles synthesized by femtosecond laser ablation and irradiation", *RSC Adv.,* 9(3) (2019) 1517-1525.

[10] W.K. Abad, W.S. Abdul Wahab and A.N. Abd, "Preparation copper iodide by laser ablation method and investigation of its effect in biomedicine", *AIP Conf. Proc*., 3282(1) (2025)

050043.
[11] I.Y. Khairani et al., "Green nanoparticle synthesis at scale: a perspective on overcoming the limits of pulsed laser ablation in liquids for high-throughput production", *Phys. Chem. Chem. Phys.,* 25(29) (2023) 19380-19408.
[12] V. Amendola and M. Meneghetti, "What controls the composition and the structure of nanomaterials generated by laser ablation in liquid solution?", *Phys. Chem. Chem. Phys.,* 15(9) (2013) 3027-3046.
[13] D. Zhang, Z. Li and K. Sugioka, "Laser ablation in liquids for nanomaterial synthesis: Diversities of targets and liquids", *J. Phys.: Photon.,* 3(4) (2021) 042002.
[14] S. Shafiei, "Optical properties of AgI nanoparticles for cloud seeding", *J. Phys.: Conf. Ser*., 2970(1) (2025) 012008.
[15] A. Sakthisabarimoorthi et al., "Fabrication of Cu@Ag core–shell nanoparticles for nonlinear optical applications", *J. Mater. Sci.: Mater. Electron.,* 28(6) (2017) 4545-4552.
[16] M.Y. Ali et al., "Vanadium Pentoxide and Bismuth Oxide Thin Films Deposition on PSi for Application in Solar Cells", *Silicon,* 17(3) (2025) 625-634.
[17] M.A. Alkhalayfeh et al., "Plasmonic effects of Au@Ag nanoparticles in buffer and active layers of polymer solar cells for efficiency enhancement", *Materials,* 15(16) (2022) 5472.
[18] T.R. da Costa et al., "Fe_3O_4@C core-shell nanoparticles as adsorbent of ionic zinc: evaluating of the adsorptive capacity", *Mater. Res.,* 22 (2019) e20180847.
[19] S.M. Feyadh and A.H. Mohammed, "The antimicrobial activity of silver & silver iodide nanoparticles synthesized via chemical reduction method", *Jundishapur J. Microbiol.,* 15(1) (2022) 1969-1988.
[20] B.P. Rakgalakane and M.J. Moloto, "Aqueous Synthesis and Characterization of CdSe/ZnO Core-Shell Nanoparticles", *J. Nanomater.,* 2011(1) (2011) 514205.
[21] A. Farzaneh et al., "Cesium-iodide-based nanocrystal for the detection of ionizing radiation", *Opt. Mater.*, 55 (2016) 22-26.
[22] A.N. Abd, M.F. Al Marjani and Z.A. Kadham, "Synthesis of CdO NPs for antimicrobial activity", *Int. J. Thin Films Sci. Technol.,* 7(1) (2018) 43-47.
[23] N.F. Habubi et al., "Improved photoresponse of porous silicon photodetectors by embedding CdSe nanoparticles", *Indian J. Pure Appl. Phys.,* 53 (2015) 718-724.
[24] J.A. Saimon et al., "Ag@WO_3 core–shell nanocomposite for wide range photo detection", *Sci. Rep.,* 14(1) (2024) 28192.
[25] C.-H. Lin and C.W. Liu, "Metal-insulator-semiconductor photodetectors", *Sensors,* 10(10) (2010) 8797-8826.
[26] W.M. Mohammd et al., "Enhanced Broadband Photo-detection via Carbon Nanotube Integration in ZnO Nanostructured Films", *Physica B: Cond. Matter,* 716 (2025) 417655.

Table (1) Parameters obtained from the X-ray diffraction patterns of AgI and Cu@AgI samples

Sample	Position (deg)	d-spacing (Å)	Height (cts)	FWHM (deg)	Crystallite size (nm)	Average crystalline size (nm)
AgI	23.4588	3.77328	508.2437	0.3936	19.75	39.720
	28.14435	3.10587	378.4508	0.0984	78.28	
	32.59854	2.8185	350.1079	0.1968	38.72	
	39.35232	2.28966	161.8058	0.3936	18.99	
	74.21472	1.27976	48.88472	0.1476	42.90	
AgI@Cu	23.49205	3.75651	497.5388	0.3936	19.75	31.721
	26.99122	3.45888	447.3283	0.1476	52.31	
	28.59008	3.12335	297.6323	0.1968	39.10	
	29.35835	3.0423	302.5029	0.1968	39.03	
	32.01522	2.82139	202.9005	0.2952	25.85	
	39.54226	2.28076	81.92624	0.1968	37.97	
	74.19003	1.3155	24.94432	0.7872	8.04	

